ORIGINAL ARTICLE

Functional significance of post-myocardial infarction inflammation evaluated by 18F-fluorodeoxyglucose imaging in swine model

Xiao-Ying Xi, MD,[a] Feifei Zhang, MD,[b] Jianfeng Wang, MD,[b] Wei Gao, MD,[c] Yi Tian, MD,[d] Hongyu Xu, MD,[e] Min Xu, MD,[f] Yuetao Wang, MD,[b] and Min-Fu Yang, MD[a]

[a] Department of Nuclear Medicine, Beijing Chaoyang Hospital, Capital Medical University, Beijing, China
[b] Department of Nuclear Medicine, The Third Affiliated Hospital of Soochow University, Changzhou, Jiangsu, China
[c] Department of Ultrasound, Beijing Chaoyang Hospital, Capital Medical University, Beijing, China
[d] Department of Nuclear Medicine, Beijing Anzhen Hospital, Capital Medical University, Beijing, China
[e] Department of Pathology, Fuwai Hospital, The National Center for Cardiovascular Diseases, Chinese Academy of Medical Sciences and Peking Union Medical College, Beijing, China
[f] Department of Echocardiogram, The Third Affiliated Hospital of Soochow University, Changzhou, Jiangsu, China

Background. The aim of the study was to investigate the relationship between post-myocardial infarction (MI) inflammation and left ventricular (LV) remodeling in a swine model by 18F-fluorodeoxyglucose (FDG) imaging.

Methods. MI was induced in swine by balloon occlusion of the left anterior descending coronary artery. A series of FDG positron emission tomography (PET) images were taken within 2 weeks post-MI, employing a comprehensive strategy to suppress the physiological uptake of cardiomyocytes. Echocardiography was applied to evaluate LV volume, global and regional function. CD68$^+$ macrophage and glucose transporters (GLUT-1, -3 and -4) were investigated by immunostaining.

Results. The physiological uptake of myocardium was adequately suppressed in 92.3% of PET scans verified by visual analysis, which was further confirmed by the minimal expression of myocardial GLUT-4. Higher FDG uptake was observed in the infarct than in the remote area and persisted within the observational period of 2 weeks. The FDG uptake of infarcted myocardium on day 1 post-MI was correlated with LV global remodeling, and the FDG uptake of infarcted myocardium on days 1 and 8 post-MI had a trend of correlating with regional

Xiao-Ying Xi and Feifei Zhang have contributed equally to this work and are co-first.

Reprint requests: Yuetao Wang, MD, Department of Nuclear Medicine, The Third Affiliated Hospital of Soochow University, No. 185, Juqian Street, Changzhou, Jiangsu 213003, China; *yuetao-w@163.com*; Min-Fu Yang, MD, Department of Nuclear Medicine, Beijing Chaoyang Hospital, Capital Medical University, 8th Gongtinanlu Rd, Chaoyang District, Beijing 100020, China; *minfuyang@126.com*

remodeling of the infarct area.

Conclusions. We here report a feasible swine model for investigating post-MI inflammation. FDG signal in the infarct area of swine persisted for a longer duration than has been reported in small animals. FDG activity in the infarct area could predict LV remodeling. (J Nucl Cardiol 2020;27:519–31.)

Key Words: FDG • PET • Myocardial infarction • Inflammation

Abbreviations	
MI	Myocardial infarction
GLUT	Glucose transporter
FDG	Fluorodeoxyglucose
LV	Left ventricular
SPECT	Single photon emission computed tomography
PET/CT	Positron emission tomography/computed tomography
SUV	Standardized uptake value
EDV	End-diastolic volume
ESV	End-systolic volume
EF	Ejection fraction
GLS	Global longitudinal strain
ILS	Infarct area longitudinal strain

INTRODUCTION

Acute myocardial infarction (MI) provokes a persistent inflammatory process that is characterized by the infiltration of a mass of leukocytes and monocytes/macrophages in the infarcted area.[1,2] These mononuclear phagocytes play a crucial role in the healing of MI. Two phases of the inflammatory process after acute MI have been validated, phagocytic and proteolytic function dominate in the first phase, while healing via myofibroblast accumulation, angiogenesis, and deposition of collagen mostly take place later.[3–7] Studies have suggested that well-balanced monocyte recruitment and activation would promote the proper healing of ischemic injury. Excessive or abolished monocytes/macrophages could bring about infarct expansion, contractile dysfunction, and heart failure, finally resulting in a poor clinical outcome.[8–10] Therefore, the evaluation of post-MI inflammation has important clinical significance, but currently there are no effective methods suitable for clinical use.

Due to the upregulation of the membrane glucose transporters (GLUTs) and acceleration of glycolytic activity in immunocytes, increased glucose metabolism may be useful for reflecting inflammatory cell recruitment. Therefore, ^{18}F-fluorodeoxyglucose (FDG) imaging has recently been applied to assess the degree of inflammation after MI.[11–14] However, the variable extent of the physiological uptake of FDG in cardiomyocytes may affect precise evaluation of the inflammatory response. Although several relevant strategies[15] have been clinically used to suppress the physiological uptake of cardiomyocytes, they have only limited success in preclinical imaging with rodents. Whether these strategies work in swine, a common large-animal model for MI study, is still unknown.

Furthermore, although the general inflammatory pathways and cell types are similar across species, the time course of inflammation differs between large and small animals after MI. Post-MI inflammation in large animals is more progressive and sustained, and more similar to that in humans.[16] However, the current time course of post-MI inflammation was mostly derived from small animal studies, which might not be translatable to human studies. Therefore, it is crucial to perform serial PET studies on large animals to determine the optimal imaging point, since that was not justified in humans.

Several studies have investigated the relationship between FDG activity in either infarct or remote areas and left ventricular (LV) remodeling. Rischpler et al.[13] demonstrated that the FDG signal in the infarct myocardium on day 5 after MI was inversely correlated with LV function at 6 months. By contrast, Wollenweber et al.[14] proposed that patients with a higher metabolic rate of glucose in the infarct area early after MI tended to have better clinical outcomes. Thus, the issue of whether FDG signal of the infarct area has a protective or detrimental effect on LV functional outcome is still debatable. It has been confirmed that the remote myocardium also has infiltration of inflammatory cells after acute MI. Several previous studies have shown an association between the tissue characteristics of remote area and reverse myocardial remodeling.[17–20] However, inflammation in the remote area has been less studied, and its relationship with LV remodeling warrants further study.

Therefore, the aims of this study were as follows: (1) to verify the efficiency of a clinically used cardiomyocyte suppression strategy in a swine model, (2) to assess dynamic change of myocardial inflammation after MI, and (3) to assess functional significance of post-MI inflammation in the infarct and remote areas.

METHODS

Animals

The animal experiments were conducted in accordance with the Declaration of Helsinki, with the guide for care and use of laboratory animals and with the approval of the Animal Ethics Committee of Soochow University. Male Bama miniature swine ($n = 20$; 35-40 kg) 6 months old were obtained from the Academy of Agricultural Sciences, Jiangsu, China and confirmed to be healthy.

Study Design

Figure 1 shows the flowchart of the study. Swine were divided into three groups: group 1 ($n = 10$), MI model with serial imaging and functional evaluation for 4 weeks (days 1, 8 and 28), group 2 ($n = 6$), MI model for imaging and pathological study (days 1, 5, 8 and 14), and group 3 ($n = 4$), sham-operation model for imaging and pathological study (days 1 and 5). Moreover, baseline perfusion imaging, echocardiography or FDG imaging was conducted respectively as normal control. One swine in group 1 died of ventricular fibrillation during the operation.

Model of Myocardial Infarction

MI was created via percutaneous transluminal coronary balloon occlusion, as described in previous studies.[21,22] Briefly, the swine were intramuscularly sedated with ketamine (35 mg·kg^{-1}) and induced with diazepam (1.5 mg·kg^{-1}). Once the swine were immobilized, maintenance anesthesia was initiated through the intravascular injection of propofol (4-

6 mL/hour). The right femoral artery and vein were exposed and isolated, and then a 7F introducer was placed. A dilation catheter was delivered to the appointed place immediately after the origin of the first diagonal branch of the left anterior descending coronary artery. A balloon was kept inflated for 90 minutes to occlude all of the blood flow distal to the balloon. Coronary occlusion was confirmed by coronary angiography. Then, the balloon was slowly deflated, and reperfusion was displayed by angiography (Figure 2A). Vital parameters such as pulse oximetry, heart rate, blood pressure, temperature and respiratory rate were monitored throughout the surgery. In the sham-operation group, the procedure was the same as that in the MI group except that the balloon was not dilated.

Myocardial Perfusion Imaging

^{99m}Tc-sestamibi myocardial perfusion imaging (MPI) was performed in group 1 at baseline and days 1, 8 and 28 for MI confirmation and localization. Tomographic acquisition was performed 45 minutes after administration of ^{99m}Tc-sestamibi using a dual-head single photon emission computed tomography (SPECT)/CT scanner (Symbia T16; Siemens Medical Systems, Erlangen, Germany) equipped with a low-energy, high-resolution collimator. The angle between the two detectors was 90°. Perfusion images were acquired every 35 s, 6° per view, with an acquisition matrix of 128×128 and a zoom factor of 1.45. Images were reconstructed by standard filtered back projection with a Butterworth filter (cut-off frequency, 0.35 cycles/cm; order, 5.0) and displayed as short-axis, vertical and horizontal long-axis slices (Figure 3A).[22] Notably, MPI on days 1 and 8 post-MI was performed before positron emission tomography/computed tomography (PET/CT) imaging.
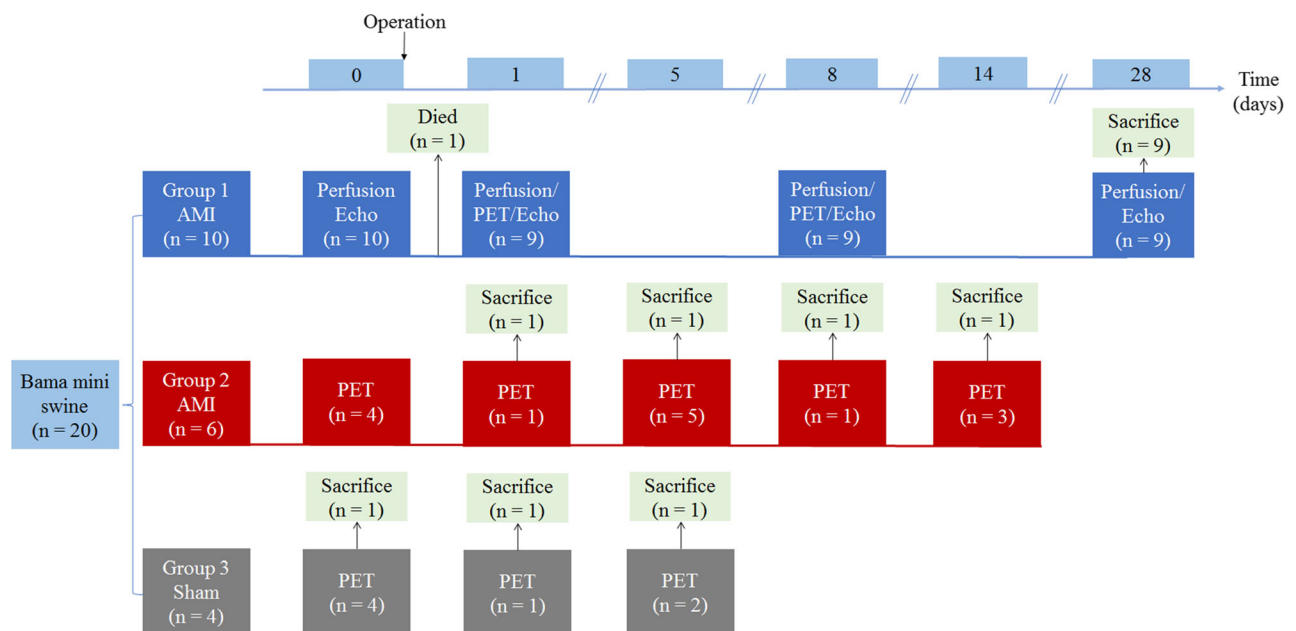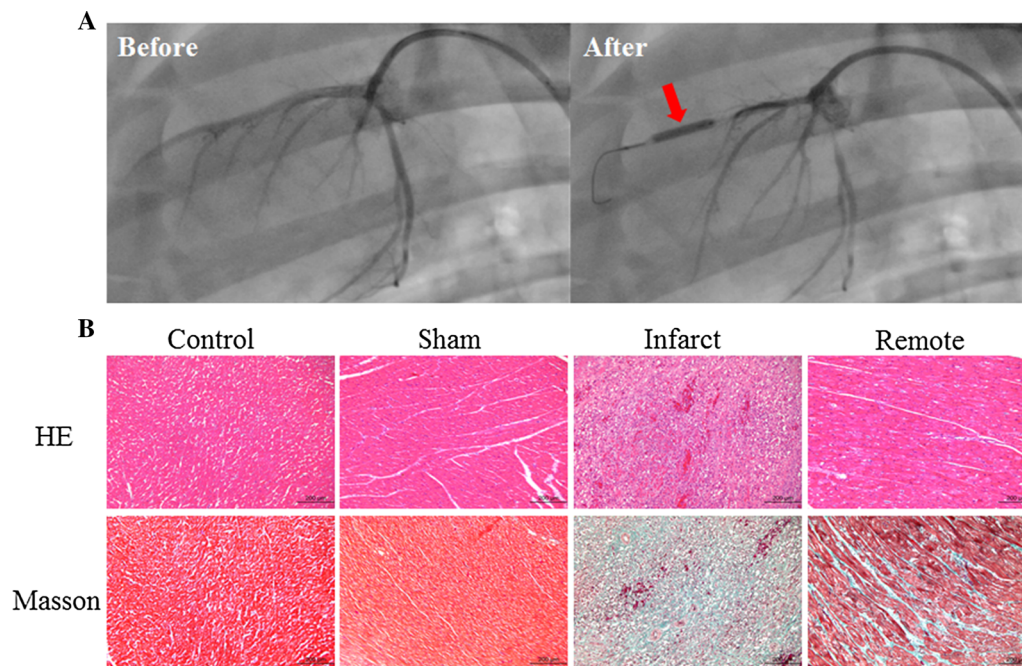

Figure 1. Study flow chart. *PET* positron emission tomography, *Echo* echocardiography.

Figure 2. Coronary angiography before (**A**, left) and after (**A**, right) balloon occlusion. The red arrow indicates the balloon. **B** HE and Masson staining of the myocardium on day 5 post-MI. The infarct area showed widespread necrosis of myocytes, large amounts of inflammatory cell infiltration, abundant collagen deposition and rare viable myocardium. The remote area displayed little collagen deposition. *HE* hematoxylin–eosin.

FDG Imaging

Acquisition To suppress physiological uptake of FDG in cardiomyocytes, all swine received a low-carbohydrate diet the day before imaging followed by a 12-hour fasting. Unfractionated heparin (50 IU·kg^{-1} body weight) was intravenously administered 15 minutes before FDG injection.[14] Propofol was injected into the auricular vein for maintenance anesthesia, and FDG (5 to 8 MBq·kg^{-1}) was administered 1 hours before PET/CT (Biograph 64; Siemens Medical Systems, Erlangen, Germany) scanning. After a scout CT acquisition (120 kV, 10 mA) used for heart positioning, CT transmission scanning (140 kV, 35 mA) was performed for attenuation correction and anatomical localization. A PET scan was acquired immediately after CT scanning, and the scanning time was set to 10 minutes. PET/CT images were reconstituted using a 3D ordered-subset expectation maximization (3D-OSEM) algorithm (21 subsets, 2 iterations) as previously described.[23]

Image fusion FDG and MPI images were processed with cardiac dedicated software QGS/QPS (version 3.1; Cedars-Sinai Medical Center, Los Angeles, CA, US) and displayed in short-axis, vertical and horizontal long-axis slices. Polar maps were automatically generated. FDG and MPI images were manually co-registered (Figure 3A).

Image analysis First, adequacy of myocardial suppression was evaluated using a 3-grade scoring system[15]: grade

A, excellent myocardial suppression with myocardial uptake lower than blood pool activity; grade B, moderate myocardial suppression with diffuse low-level myocardial FDG uptake and nonspecific focally increased uptake in papillary muscles and lateral wall; grade C, poor myocardial suppression with regional or diffuse high-level FDG uptake. Grade A was thought to be adequately suppressed.

Thereafter, FDG images were quantitatively analyzed using the commercial software package MedEx (MedEx Technology Co. Ltd., Beijing, China). Volume of interest (VOI) was determined by a region grow algorithm with a threshold of 50% of the maximum uptake. The maximum standardized uptake value (SUV$_{max}$) of the infarct region was measured from the VOI. The mean standardized uptake value (SUV$_{mean}$) in the remote myocardium (mid-inferior wall) was obtained by manually drawn regions in the inferior wall on three consecutive slices oriented by PET/CT fusion image. SUV$_{mean}$ in the normal-control and sham-operation group was obtained by manually drawn regions in the anterior and inferior walls on three consecutive slices oriented by PET/CT fusion image.

All image processing and interpretation were independently performed by two experienced nuclear medicine physicians (XYX and MFY), and any disagreements were resolved by consensus.
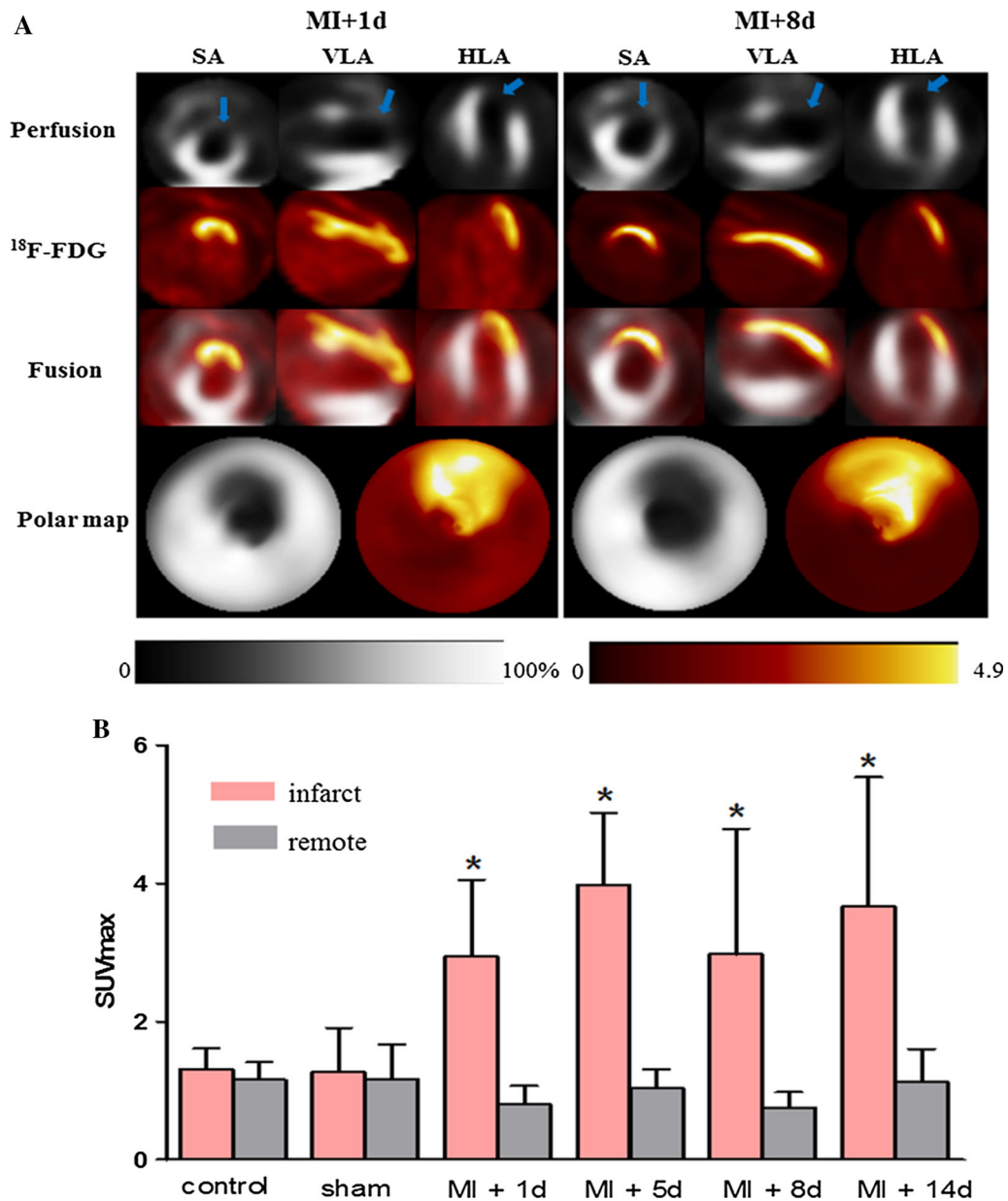
Figure 3. A An example of serial post-MI myocardial imaging. Arrows indicate infarct zone. **B** Quantitative comparison of SUV. $*P < .05$ indicates comparison with the remote area of MI group, normal-control or sham-operation group. *SA* short-axis, *VLA* vertical long-axis, *HLA* horizontal long-axis, *[18]F-FDG* ^{18}F-fluorodeoxyglucose, *SUV_{max}* maximum standardized uptake value.

Echocardiography

Left ventricular functional analysis Transthoracic echocardiography was performed using commercially available ultrasound systems (EPIQ 7C; Philips Healthcare, Andover, MA, USA). LV end-diastolic volume (LVEDV) and LV end-systolic volume (LVESV) were calculated using the Simpson biplane method of disks. LV ejection fraction (LVEF) was calculated and expressed as a percentage.

ΔEDV, ΔESV and ΔEF are expressed as a change ratio of EF, EDV and ESV between days 1 and 28 post-MI.

Myocardial strain analysis Speckle-tracking echocardiography was employed to quantify longitudinal myocardial function, which was measured offline in the three apical (2-, 3-, and 4-chamber) views using Philips QLAB v10.0 software (Philips Healthcare). During image analysis, the LV endocardial border was manually traced at the end-systole, and the region-of-interest width was adjusted to include the entire

myocardium. The software automatically tracks myocardial speckle patterns frame by frame during one cardiac cycle (R-R interval) and generates LV strain parameters for each of the 17 segments (Figrue 4). The global longitudinal strain (GLS) was obtained automatically. The infarct area longitudinal strain (ILS) was calculated as the mean value of the longitudinal strain in the infarcted segment determined by MPI. ΔGLS and ΔILS are expressed as change ratios of GLS and ILS between days 1 and 28 post-MI.

Histological Assessments

Swine were sacrificed while under anesthesia immediately after the imaging was completed. The heart was quickly removed and rinsed with saline. Myocardial tissue was obtained from the anterior wall (infarct area) and inferior wall (remote area) at the middle level of the left ventricle for each heart and fixed in 10% formalin. All tissue samples were embedded with paraffin and prepared as 5 μm-thick sections. Then, these sections were stained with hematoxylin–eosin (HE) and Masson to confirm the success of MI modeling and observe morphological changes in myocardial tissues. Immunohistochemistry was applied to identify the CD68$^+$ macrophage population and expression of GLUT-1, GLUT-3 and GLUT-4 according to a standard immunostaining procedure. Briefly, deparaffinized sections were incubated with anti-CD68 (Zhongshan biotechnology co. LTD, Beijing, China) or anti-GLUT antibodies (Synaptic Systems, Göttingen, Germany) for 30 minutes at 37 °C. The bound antibody was visualized using the avidin/biotin conjugate immunoperoxidase procedure and 3,3′-diaminobenzidine tetrahydrochloride. HE and Masson images were displayed at ×100 magnification; CD68$^+$ and GLUT images were displayed at ×400 magnification.

For the evaluation of macrophages, 10 independent × 400 microscopic fields were randomly selected from CD68$^+$ immunohistochemical staining slices. The total number of positively stained cells per 10 microscopic fields was counted.

For the evaluation of GLUTs, 10 independent × 400 microscopic fields were randomly selected from each of the GLUTs immunohistochemical staining slices. According to the criteria of Higashi et al.,[24] staining intensity was scored from 0 to 3 (0, not stained; 1, equivocal; 2, intense; and 3, very intense). And, percentage of positively stained cells was scored from 1 to 5 (1, 0%-20%; 2, 21%-40%; 3, 41%-60%; 4, 61%-80%; and 5, 81%-100%). The expression of GLUTs was determined by the product of staining intensity and percentage of positively stained cells.[25]

Statistical Analysis

Statistical analyses were performed using SPSS version 19.0 (SPSS, Chicago, IL, USA) and GraphPad Prism version 5.01 (GraphPad Software Inc., San Diego, CA, USA). Continuous variables are expressed as mean ± standard deviation and were compared using a two-tailed Student's t-test. The association between continuous variables was explored using the Pearson correlation coefficient. Categorical variables are expressed as absolute numbers or percentages. $P < .05$ was considered to be statistically significant.
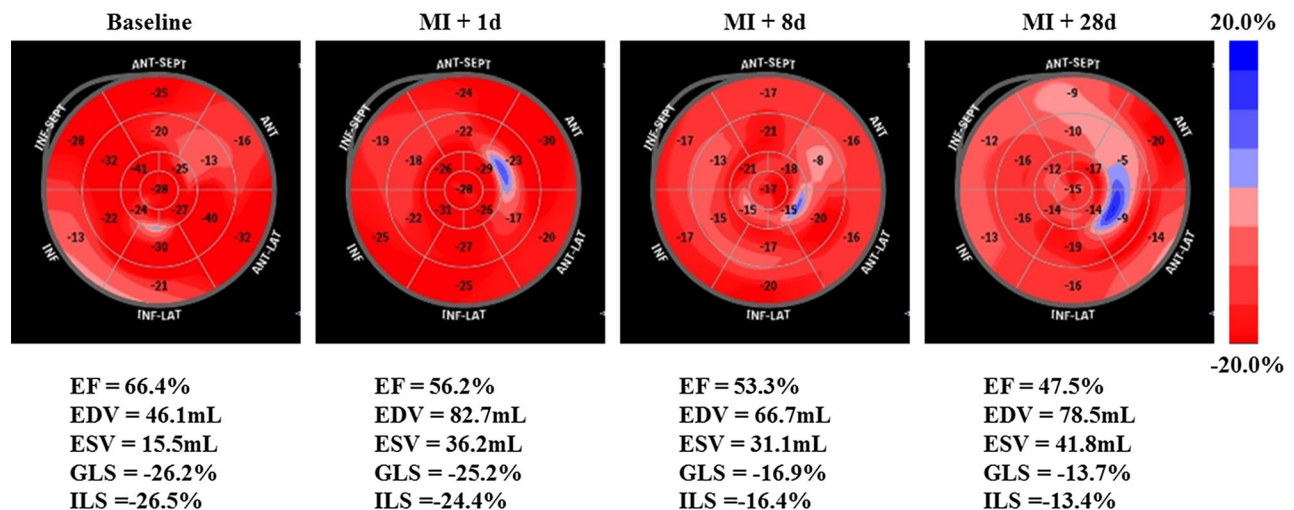
Figure 4. An example of serial speckle-tracking images of MI swine. The value of GLS and ILS gradually decreased after MI. *GLS, global longitudinal strain; ILS, infarct area longitudinal strain; EF, ejection fraction; EDV, end-diastolic volume; ESV, end-systolic volume.*

RESULTS

Animal Model

MI was verified by HE and Masson staining displaying widespread necrosis of myocytes, inflammatory cell infiltration and abundant collagen deposition in the infarct area (Figure 2B). Furthermore, MPI of the MI swine model showed perfusion defects in the anterior wall, anteroseptal wall and apex of the left ventricle, consistent with left anterior descending coronary artery domination (Figure 3A).

Myocardial FDG Uptake

With diet and heparin pretreatment, the physiological uptake of cardiomyocytes was adequately suppressed in 92.3% (36/39) FDG scans. For the baseline imaging, one scan with inadequate suppression was excluded from subsequent analysis. For the MI imaging, FDG uptake in the remote area was slightly higher than in the infarct area in 1 PET scan (SUV: 1.9 vs 1.8), making it difficult to distinguish between inflammation and physiological uptake. Another PET scan showed strong physiological uptake in the remote area (SUV$_{mean}$: 13.3), which was considered failure of physiological-uptake suppression. These two PET scans were also excluded from subsequent analysis.

For the remaining PET scans, the SUV$_{max}$ in the infarct area was significantly higher than in the remote area (Figure 3B). However, the SUV$_{mean}$ of the remote area in MI was not different from that of the normal-control and sham-operation groups. Notably, there was no significant change in FDG uptake in either the infarct or the remote area within 14 days post-MI.

Macrophage Recruitment and GLUT Expression

Immunostaining demonstrated robust recruitment of CD68$^+$ macrophages to the infarct area. There were also a few CD68$^+$ macrophages recruited to the remote area, compared with the normal-control and sham-operation groups (Figure 5A). However, the number of CD68$^+$ macrophages in either the infarct or the remote area did not change with visual analysis within 14 days post-MI (Figure 5B).

There was a high intensity of GLUT-1 and GLUT-3 in the infarct area, which was 3.00-3.83 folds higher than that in the remote area. The expression of GLUT-1 and GLUT-3 in the infarct area was 3.45-4.99 folds higher than the expression of GLUT-4 (Figure 6). The expression of GLUTs in the infarct area was dominantly in the infiltrated inflammatory cells. The expression of GLUT-4 was minimal in the remote myocardium and no different from that in the normal-control and sham-operation groups (Figure 6). The expression of GLUTs in either the infarct or the remote area did not change within 14 days post-MI (Figure 6B).

Relationship Between FDG Uptake and Myocardial Remodeling

Global analysis Serial analysis of LV function showed a decrease in EF, increase in EDV and ESV and no change in GLS between days 1 and 28 post-MI (Figure 7A-D). There was no correlation between the SUV$_{max}$ of the infarct area on day 1 or 8 post-MI and ΔEF, ΔEDV or ΔESV (Table 1). However, ΔGLS had a negative correlation with the SUV$_{max}$ of the infarcted myocardium on day 1 post-MI ($r = -0.717$, $P = .030$; Figure 8A and Table 1).

Regional analysis Post-MI ILS showed a significant decrease compared with that at baseline. However, there was no change in ILS from days 1 to 28 post-MI (Figure 7E). In addition, ΔILS tended to inversely correlate to the SUV$_{max}$ of the infarct area on days 1 and 8 post-MI (day 1: $r = -0.589$, $P = .095$; day 8: $r = -0.602$, $P = .086$; Figure 8B, C and Table 1).

DISCUSSION

The main findings of this study were threefold: (1) increased FDG signal in the infarct area persisted for 2 weeks post-MI; (2) the intensity of FDG activity in the infarct area could predict LV remodeling; and (3) the clinically used strategy for cardiomyocyte suppression was effective in swine, which was firstly verified by evaluating myocardial GLUT expression.

Dynamic Changes of Post-MI FDG Activity

In a retrospective clinical study, Wollenweber et al.[14] first demonstrated an increased glucose uptake in the infarcted myocardium and an association between glucose uptake in the infarcted myocardium and activation of lymphoid tissue in the spleen and bone marrow in human beings. In another study, Lee and his colleagues[12] suggested that inflammatory response in the infarct area peaks around 5 days post-MI in a mice model. In contrast with Lee et al.'s study, there were no significant fluctuation of FDG activity and GLUTs expression in the infarct area within 14 days post-MI in our study. The temporal difference in post-MI inflammation might be mainly attributable to the difference in research model between swine and mice. As swine are physiologically close to humans, the time course of post-

A

Control MI + 5d (Infarct)

Sham MI + 5d (Remote)

B
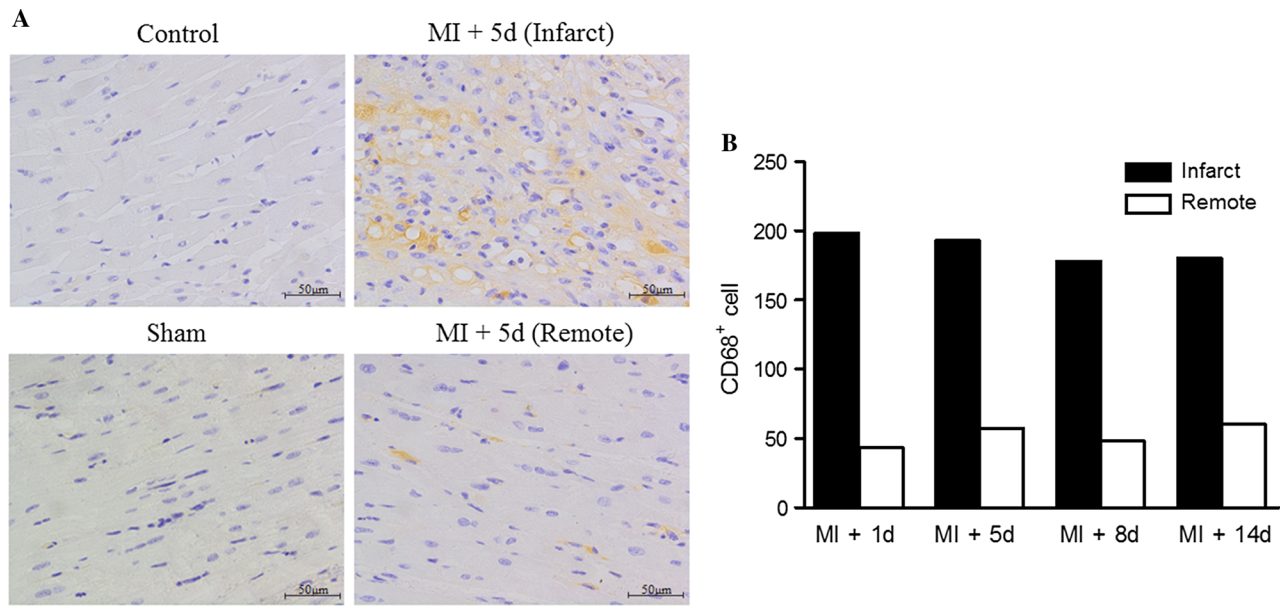
Figure 5. A CD68$^+$ staining of the myocardium on day 5 post-MI. There were apparent macrophages accumulation in the infarct area and scarce macrophages in the remote area. **B** Semi-quantitative comparison of CD68$^+$ macrophages within 14 days post-MI. The number of CD68$^+$ macrophages in either the infarct or the remote area did not change within 14 days post-MI.

MI inflammation in swine indicated that the imaging window for MI patients could be widened.

Functional Significance of FDG Activity in the Infarct Myocardium

In a pioneering prospective study, Rischpler et al.[13] investigated the value of FDG PET/MRI imaging in predicting functional outcome in patients with MI. Their results showed that a higher SUV$_{mean}$ in the infarct area on day 5 after infarction could predict worsening LVEF after 6 months. In our study, although we did not observe a relationship between FDG uptake in the infarct area and ΔEF, ΔEDV or ΔESV, we found that ΔGLS had a negative correlation with the SUV$_{max}$ of the infarct area on day 1 post-MI. From this point forward, our findings were partially consistent with Rischpler's.

Lee et al.[12] found that matrix metalloproteinase activity was significantly increased in non-infarcted myocardium, suggesting that monocyte recruitment to the remote area may contribute to post-MI dilation. Wollenweber et al.[14] indicated that patients with higher metabolic rate of glucose in the remote myocardium showed a trend toward a worse clinical outcome. Rischpler et al.[13] found that there was no correlation between FDG uptake in the remote myocardium and changes in cardiac function. In our study, although Masson and CD68$^+$ staining showed a small amount of collagen deposition and macrophage infiltration in the remote area, there was no significant difference in FDG uptake among the remote area of MI group, normal-control and sham-operation groups, which prevented us from further analyzing its functional significance. The possible reasons for this lack of difference were as follows: (1) inflammatory response in the remote area was too weak to be detected by FDG PET; and (2) physiological uptake of myocardium was not completely suppressed. Therefore, the functional significance of post-MI inflammation in the remote area needs to be further studied with an inflammation-specific imaging agent.

Swine Model for Assessing Post-MI Inflammation

FDG imaging has increasingly been used for investigating post-MI inflammation in preclinical and clinical settings.[11–14,26,27] Nevertheless, image preparation and interpretation remain challenging due to the unpredictable uptake of healthy cardiomyocytes. Currently, several relevant strategies have been used to suppress the physiological uptake of cardiomyocytes in animal or clinical studies, such as long periods of fasting,[27] high-fat combined with low-carbohydrate diet preparations[28,29] or heparin pre-administration.[30,31] These strategies have worked well in most human studies.
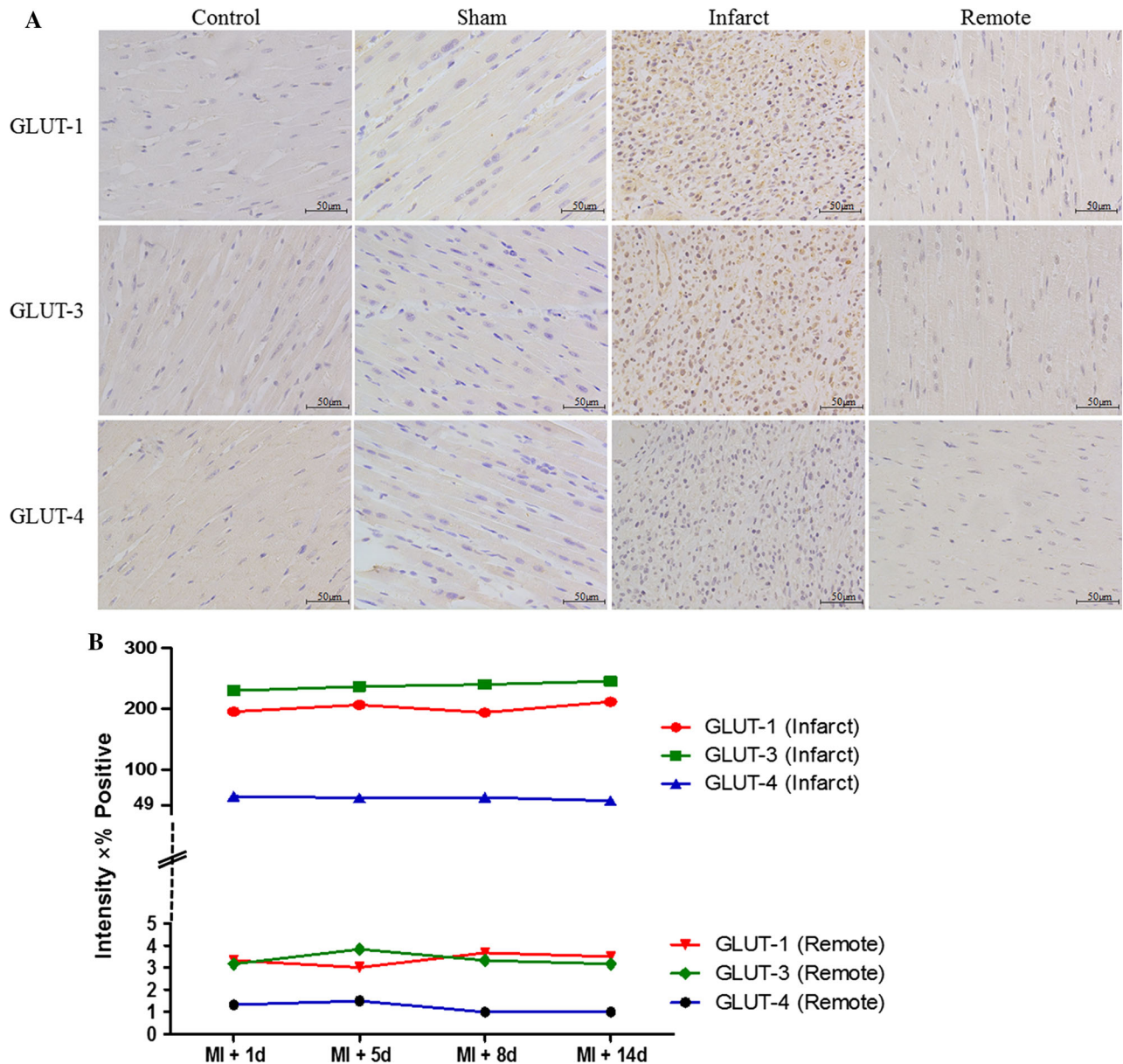
Figure 6. **A** Immunostaining of myocardial GLUTs on day 5 post-MI. Abundant GLUT-1 and GLUT-3 were expressed in the infarct area. The expression level of GLUT-4 was lower than that of GLUT-1 or GLUT-3. **B** Semi-quantitative comparison of GLUTs within 14 days post-MI. The expression level of GLUTs in either the infarct or the remote area did not change within 14 days post-MI. *GLUT* glucose transporter.

However, most anesthetics increase myocardial glucose uptake in mice,[32] which obscures the suppressive effects of the methods mentioned above.[27] Mice have therefore been proven a suboptimal model for assessing post-MI inflammation. Lautamäki et al.[26] used a swine model to investigate post-MI FDG uptake with a euglycemic hyperinsulinemic clamping preparation. Under this condition, the physiological uptake of myocardium could not be suppressed; therefore, it was not possible to

evaluate FDG uptake. In our study, for maximum inhibition of the physiological uptake of cardiomyocytes, we combined low-carbohydrate diet and long-duration fasting with heparin pre-injection. As a result, the physiological uptake of myocardium was adequately suppressed in 92.3% of PET scans, which indicated that this cardiomyocyte suppression strategy was effective in swine.
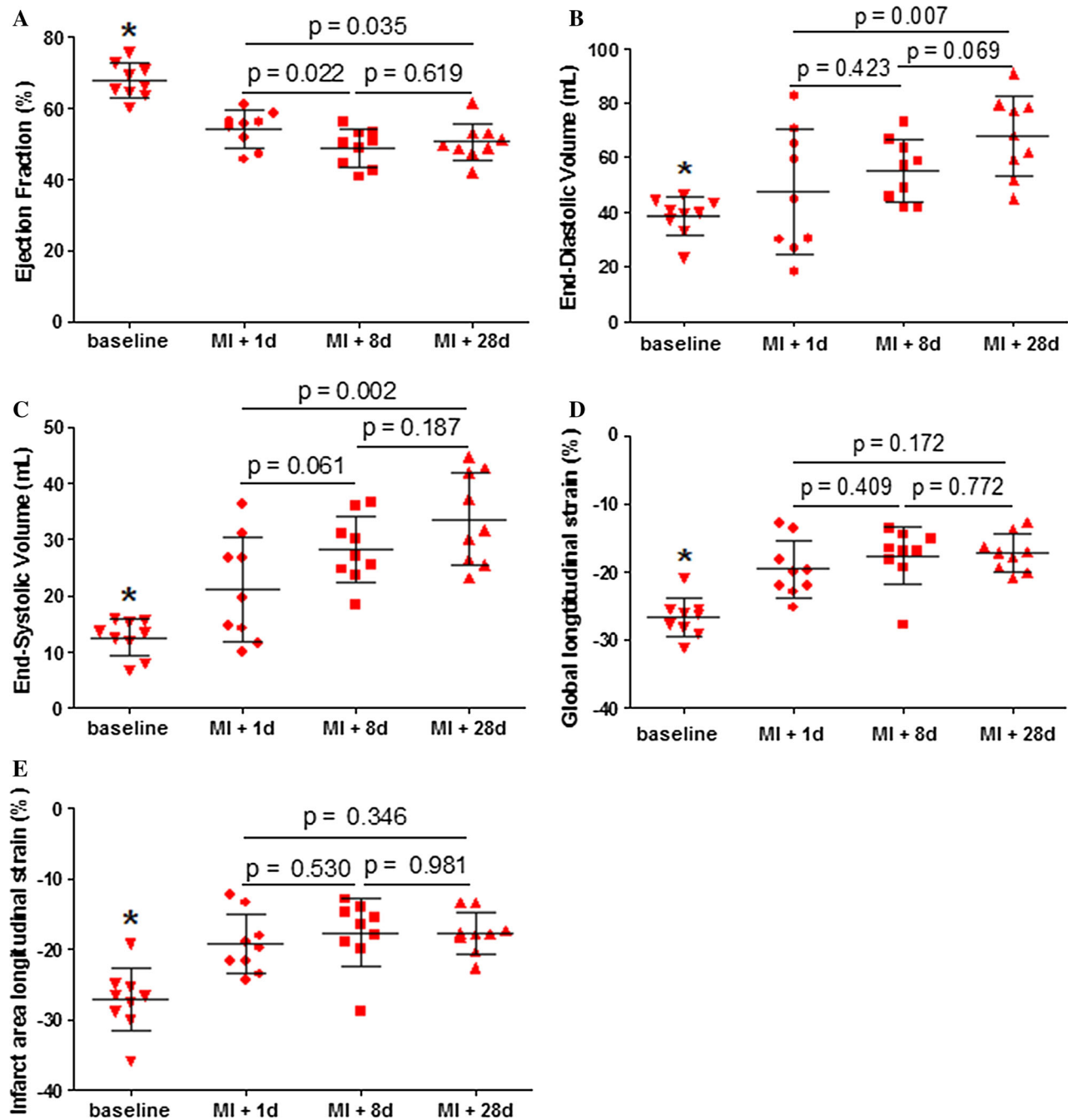
Figure 7. Changes of **A-D** LV function and **E** infarct area function (ILS) over time. *$P < .05$ between baseline and each time point post-MI. *EF* ejection fraction, *EDV* end-diastolic volume, *ESV* end-systolic volume, *GLS* global longitudinal strain, *ILS* infarct area longitudinal strain.

Normal cardiomyocytes mainly express GLUT-4; the translocation of GLUT-4 from an intracellular pool to the cell surface is the rate limiting step in glucose uptake. However, in inflammatory cells, glucose enters the cells mainly through constitutively expressed GLUT-1 and GLUT-3.[15] In our study, expression levels of GLUT-1 and GLUT-3 in the infarct area were higher than those in the remote area, and in the corresponding regions in the normal-control and sham-operation groups. By contrast, the expression of GLUT-4 was minimal in the remote myocardium and in the myocardium of the normal-control and sham-operation groups,

Table 1. Correlation between cardiac function follow-up and FDG uptake in the infarct myocardium

| LV function | SUV$_{max}$ | | | | |
| | 1 day post-MI | | | 8 day post-MI | |
	r	P		r	P
ΔEF	− 0.088	.823		− 0.124	.751
ΔEDV	− 0.582	.100		− 0.446	.229
ΔESV	− 0.546	.128		− 0.369	.328
ΔGLS	− 0.717	.030*		− 0.500	.170
ΔILS	− 0.589	.095		− 0.602	.086

LV left ventricular, *EF* ejection fraction, *EDV* end-diastolic volume, *ESV* end-systolic volume, *GLS* global longitudinal strain, *ILS* infarct area longitudinal strain, *SUV$_{max}$* maximum standardized uptake value, *MI* myocardial infarction
*Indicated $P < .05$
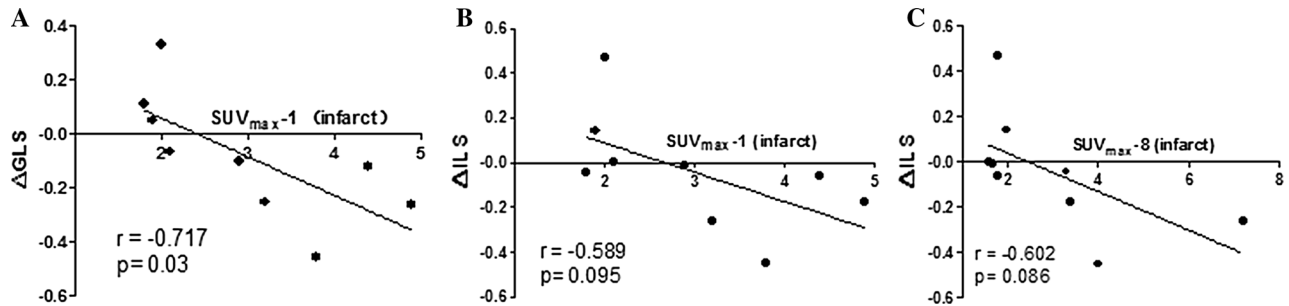
Figure 8. Correlation between post-MI FDG uptake and LV functional outcome. **A** Correlation between SUV$_{max}$ in the infarct myocardium on day 1 post-MI and ΔGLS (the change ratio of GLS between days 1 and 28 post-MI). **B, C** Correlation between SUV$_{max}$ in the infarct myocardium on day 1 or 8 post-MI and ΔILS (the change ratio of ILS between days 1 and 28 post-MI). *GLS* global longitudinal strain, *ILS* infarct area longitudinal strain, *SUV$_{max}$* maximum standardized uptake value.

and it was significantly lower than the expression of GLUT-1 and GLUT-3. Expression of GLUTs in this study elucidated the mechanism of cardiomyocyte suppression and was in accord with the results of PET imaging. Therefore, this study demonstrated that a swine animal model is suitable for assessing post-MI inflammation and for pre-clinical study.

Limitations

This work has several limitations. First, follow-up time was short. However, a previous study on swine has shown that global and regional cardiac function had already decreased significantly within 4 weeks after MI.[33] Therefore, we chose the time point of day 28 as the terminal of observation for functional outcome.

Second, the timing of PET imaging might not have been optimal. Lee et al. suggested that inflammatory response in the infarct area peaks around 5 days post-MI, while that in the remote area peaks around 10 days post-MI.[12] By contrast, our study showed no significant change in FDG uptake in the infarct or remote area within 14 days post-MI. The time course of inflammation in Lee et al.'s study was obtained from mice; there is a temporal difference between small and big animals, as described above. Third, a slight difference in transmural degree of MI could affect FDG uptake and LV remodeling, although perfusion imaging revealed a transmural MI in all MI swine. Fourth, although CD68^{+} immunostaining can identify macrophages, it cannot distinguish subtypes thereof. Therefore, we could not clarify the corresponding macrophage subtype of FDG uptake at

each time point. Finally, MPI and FDG images were acquired using separate camera systems and manually co-registered; therefore, imprecise fusion was inevitable.

CONCLUSIONS

A swine MI model with suppression of cardiomyocyte physiological uptake is suitable for investigating post-MI inflammation. The post-MI inflammatory response persisted longer than that has been observed in mice. FDG signal in the infarct area was related to myocardial remodeling.

NEW KNOWLEDGE GAINED

FDG intensity in the infarcted myocardium, a marker of inflammation, was related to myocardial remodeling. However, whether FDG imaging can be used to detect inflammation in the remote myocardium warrants further study. The long duration of post-MI inflammation in swine indicated that the imaging window for MI patients could be widened.

Disclosures

Xiao-Ying Xi, Feifei Zhang, Jianfeng Wang, Wei Gao, Yi Tian, Hongyu Xu, Min Xu, Yuetao Wang and Min-Fu Yang have nothing to disclose.

References

1. Kempf T, Zarbock A, Widera C, Butz S, Stadtmann A, Rossaint J, et al. GDF-15 is an inhibitor of leukocyte integrin activation required for survival after myocardial infarction in mice. Nat Med 2011;17:581-8.
2. Jung K, Kim P, Leuschner F, Gorbatov R, Kim JK, Ueno T, et al. Endoscopic time-lapse imaging of immune cells in infarcted mouse hearts. Circ Res 2013;112:891-9.
3. Majmudar MD, Keliher EJ, Heidt T, Leuschner F, Truelove J, Sena BF, et al. Monocyte-directed RNAi targeting CCR3 improves infarct healing in atherosclerosis-prone mice. Circulation 2013;127:2038-46.
4. Swirski FK, Nahrendorf M. Leukocyte behavior in atherosclerosis, myocardial infarction, and heart failure. Science 2013;339:161-6.
5. Gordon S, Taylor PR. Monocyte and macrophage heterogeneity. Nat Rev Immunol 2005;5:953-64.
6. Nahrendorf M, Pittet MJ, Swirski FK. Monocytes: Protagonists of infarct inflammation and repair after myocardial infarction. Circulation 2010;121:2437-45.
7. Van der Laan AM, Ter Horst EN, Delewi R, Begieneman MP, Krijnen PA, Hirsch A, et al. Monocyte subset accumulation in the human heart following acute myocardial infarction and the role of the spleen as monocyte reservoir. Eur Heart J 2014;35:376-85.
8. Dimitrijević O, Stojcevski BD, Ignjatović S, Singh NM. Serial measurements of C-reactive protein after acute myocardial infarction in predicting one-year outcome. Int Heart J 2006;47:833-42.
9. Prondzinsky R, Unverzagt S, Lemm H, Wegener NA, Schlitt A, Heinroth KM, et al. Interleukin-6, -7, -8 and -10 predict outcome in acute myocardial infarction complicated by cardiogenic shock. Clin Res in Cardiol 2012;101:375-84.
10. White DA, Su Y, Kanellakis P, Kiriazis H, Morand EF, Bucala R, et al. Differential roles of cardiac and leukocyte derived macrophage migration inhibitory factor in inflammatory responses and cardiac remodelling post myocardial infarction. J Mol Cell Cardiol 2014;69:32-42.
11. Thackeray JT, Bankstahl JP, Wang Y, Korf-Klingebiel M, Walte A, Wittneben A, et al. Targeting post-infarct inflammation by PET imaging: Comparison of (68) Ga-citrate and (68) Ga-DOTATATE with (18) F-FDG in a mouse model. Eur J Nucl Med Mol Imaging 2015;42:317-27.
12. Lee WW, Marinelli B, van der Laan AM, Sena BF, Gorbatov R, Leuschner F, et al. PET/MRI of inflammation in myocardial infarction. J Am Coll Cardiol 2012;59:153-63.
13. Rischpler C, Dirschinger RJ, Nekolla SG, Kossmann H, Nicolosi S, Hanus F, et al. Prospective evaluation of ^{18}F-Fluorodeoxyglucose uptake in postischemic myocardium by simultaneous positron emission tomography/magnetic resonance imaging as a prognostic marker of functional outcome. Circ Cardiovasc Imaging. 2016;9:e004316.
14. Wollenweber T, Roentgen P, Schäfer A, Schatka I, Zwadlo C, Brunkhorst T, et al. Characterizing the inflammatory tissue response to acute myocardial infarction by clinical multimodality noninvasive imaging. Circ Cardiovasc Imaging 2014;7:811-8.
15. Osborne MT, Hulten EA, Murthy VL, Skali H, Taqueti VR, Dorbala S, et al. Patient preparation for cardiac fluorine-18 fluorodeoxyglucose positron emission tomography imaging of inflammation. J Nucl Cardiol 2017;24:86-99.
16. Romito E, Shazly T, Spinale FG. In vivo assessment of regional mechanics post-myocardial infarction: A focus on the road ahead. J Appl Physiol 2017;123:728-45.
17. Chan W, Duffy SJ, White DA, Gao XM, Du XJ, Ellims AH, et al. Acute left ventricular remodeling following myocardial infarction: Coupling of regional healing with remote extracellular matrix expansion. JACC Cardiovasc Imaging 2012;5:884-93.
18. Carrick D, Haig C, Rauhalammi S, Ahmed N, Mordi I, McEntegart M, et al. Pathophysiology of LV remodeling in survivors of STEMI: Inflammation, remote myocardium, and prognosis. JACC Cardiovasc Imaging 2015;8:779-89.
19. Reinstadler SJ, Stiermaier T, Liebetrau J, Fuernau G, Eitel C, de Waha S, et al. Prognostic significance of remote myocardium alterations assessed by quantitative noncontrast T1 mapping in ST-segment elevation myocardial infarction. JACC Cardiovasc Imaging 2018;11:411-9.
20. Puntmann VO, Carr-White G, Jabbour A, Yu CY, Gebker R, Kelle S, et al. Native T1 and ECV of noninfarcted myocardium and outcome in patients with coronary artery disease. J Am Cool Cardiol 2018;71:766-78.
21. McCall FC, Telukuntla KS, Karantalis V, Suncion VY, Heldman AW, Mushtag M, et al. Myocardial infarction and intramyocardial injection models in swine. Nat Protoc 2012;7:1479-96.
22. Wang J, Wang Y, Yang M, Shao S, Tian Y, Shao X, et al. Mechanical contraction to guide CRT left-ventricular lead placement instead of electrical activation in myocardial infarction with left ventricular dysfunction: An experimental study based on non-

invasive gated myocardial Perfusion imaging and invasive electroanatomic mapping. J Nucl Cardiol. 2019. https://doi.org/10.1007/s12350-019-01710-2.

23. Shao X, Wang J, Tian Y, Fan S, Zhang F, Yang W, et al. Role of gated myocardial glucose metabolic imaging in assessing left ventricular systolic dyssynchrony after myocardial infarction and the influential factors. Sci Rep. 2018;8:11178.

24. Higashi T, Tamaki N, Honda T, Torizuka T, Kimura T, Inokuma T, et al. Expression of glucose transporters in human pancreatic tumors compared with increased FDG accumulation in PET study. J Nucl Med 1997;38:1337-44.

25. Mochizuki T, Tsukamoto E, Kuge Y, Kanegae K, Zhao S, Hikosaka K, et al. FDG uptake and glucose transporter subtype expressions in experimental tumor and inflammation models. J Nucl Med 2001;42:1551-5.

26. Lautamäki R, Schuleri KH, Sasano T, Javadi MS, Youssef A, Merrill J, et al. Integration of infarct size, tissue perfusion, and metabolism by hybrid cardiac positron emission tomography/computed tomography: Evaluation in a porcine model of myocardial infarction. Circ Cardiovasc Imaging 2009;2:299-305.

27. Thackeray JT, Bankstahl JP, Wang Y, Wollert KC, Bengel FM. Clinically relevant strategies for lowering cardiomyocyte glucose uptake for ^{18}F-FDG imaging of myocardial inflammation in mice. Eur J Nucl Med Mol Imaging 2015;42:771-80.

28. Cheng VY, Slomka PJ, Ahlen M, Thomson LE, Waxman AD, Berman DS. Impact of carbohydrate restriction with and without fatty acid loading on myocardial ^{18}F-FDG uptake during PET: A randomized controlled trial. J Nucl Cardiol 2010;17:286-91.

29. Wykrzykowska J, Lehman S, Williams G, Parker JA, Palmer MR, Varkey S, et al. Imaging of inflamed and vulnerable plaque in coronary arteries with ^{18}F-FDG PET/CT in patients with suppression of myocardial uptake using a low-carbohydrate, high-fat preparation. J Nucl Med 2009;50:563-8.

30. Schatka I, Bengel FM. Advanced imaging of cardiac sarcoidosis. J Nucl Med 2014;55:99-106.

31. Minamimoto R, Morooka M, Kubota K, Ito K, Masuda-Miyata Y, Mitsumoto T, et al. Value of FDG-PET/CT using unfractionated heparin for managing primary cardiac lymphoma and several key findings. J Nucl Cardiol 2011;18:516-20.

32. Toyama H, Ichise M, Liow JS, Vines DC, Seneca NM, Modell KJ, et al. Evaluation of anesthesia effects on [^{18}F]FDG uptake in mouse brain and heart using small animal PET. Nucl Med Biol 2004;31:251-6.

33. Koudstaal S, Gho JM, van Hout GP, Jansen MS, Gründeman PF, et al. Myocardial infarction and functional outcome assessment in pigs. J Vis Exp. 2014;86:e51269.